Biol. Cybern. 86, 367–378 (2002)
DOI 10.1007/s00422-001-0293-y

Biological Cybernetics

New attractor states for synchronous activity in synfire chains with excitatory and inhibitory coupling

Arash Yazdanbakhsh[1], **Baktash Babadi**[1,2], **Shahin Rouhani**[1,3], **Ehsan Arabzadeh**[2], **Abdolhosein Abbassian**[1]

[1] School of Intelligent Systems, Institutes for Studies in Theoretical Physics and Mathematics, P.O. Box 19395, 5746 Tehran, Iran
[2] Tehran University of Medical Sciences and Health Services, Medical Faculty, Tehran, Iran
[3] Sharif University of Technology, Department of Physics, Tehran, Iran

Received: 27 July 2001 / Accepted in revised form: 23 October 2001

Abstract. In a feedforward network of integrate-and-fire neurons, where the firing of each layer is synchronous (synfire chain), the final firing state of the network converges to two attractor states: either a full activation or complete fading of the tailing layers. In this article, we analyze various modes of pattern propagation in a synfire chain with random connection weights and delta-type postsynaptic currents. We predict analytically that when the input is fully synchronized and the network is noise free, varying the characteristics of the weights distribution would result in modes of behavior that are different from those described in the literature. These are convergence to fixed points, limit cycles, multiple periodic, and possibly chaotic dynamics. We checked our analytic results by computer simulation of the network, and showed that the above results can be generalized when the input is asynchronous and neurons are spontaneously active at low rates.

1 Introduction

In recent years, the role and importance of synchrony in cortical neural assemblies has been widely investigated. Besides many empirical studies indicating the presence of synchronous activity in biological neural systems (Abeles 1991; König et al. 1995; Lachaux et al. 1999; Usrey and Reid 1999), the computational importance of synchrony in neural networks has also been a focus of interest (Hummel and Biederman 1992; Somers and Kopell 1993; Pinsky and Rinzel 1995; Hansel and Sompolinsky 1996; Lumer et al. 1997).

Synchronized firing activity in successive neural pools in a time window much less than the membrane time constant (the so-called synfire chain activity), has been detected experimentally in cortical areas of the brain (Abeles 1991; Miller 1996; Prut et al. 1998) and has also been studied through simulations (Abeles 1991; MacGregor et al. 1995; Aertsen et al. 1996; Hertz and Prügel-Bennett 1996; Postma et al. 1996; Arnoldi et al. 1999).

Being a relatively close approximation to the biological neuron, the *integrate-and-fire* neuron (IFN) model is a good choice for studying computational properties of biological neural systems – such as synchrony – by means of simulation (Gerstner and van Hemmen 1992; Niebur and Koch 1994; Herrmann et al. 1995; Hopfield and Herz 1995; Arnoldi and Brauer 1996; Horn and Opher 1997; Rudd and Brown 1997; Tal and Schwartz 1997; Hansel et al. 1998; Kempter et al. 1998; Lin et al. 1998; Burkitt and Clark 1999; Campbell et al. 1999; Deco and Schürmann 1999).

As it has been shown in various simulations (Gerstner and van Hemmen 1992; Herrmann et al. 1995; Pinsky and Rinzel 1995; Arnoldi et al. 1996; Hertz and Prügel-Bennett 1996; Marsalek et al. 1997; Rudd and Brown 1997; Hansel et al. 1998; Kempter et al. 1998; Campbell et al. 1999; Deco and Schürmann 1999), in a multilayered feedforward neural network, consisting of IFN models, synchronous firing can be achieved in successive layers, even if the feeding input of the network is not synchronized itself.

The effect of the synchronization on the firing rate of the neural population has been investigated in a few studies (Chawla et al. 1999; Diesmann et al. 1999; Litvak et al. 2000). In a feedforward network of IFN models, a more synchronous firing of the neurons in one layer will feed the neurons in the next layer with a higher input within a narrower time band. This will happen due to the increased number of synchronous signals, which travel from layer to layer. Thus, in the presence of increasing synchronization in successive layers, one might conclude that the proportion of firing neurons will also increase successively, resulting in the firing of all neurons in the terminating layers of the network. On the other hand, if the input is not strong enough to survive during its propagation through successive layers, no firing is expected in the terminating layers. In this context, Diesmann et al. (1999) have shown that the integrate-

Correspondence to: A. Yazdanbakhsh
(e-mail: yazdan@ipm.ir,
Tel.: +98-21-2294035, Fax: +98-21-2290151)

and-fire feedforward network, fed by temporal patterns, results in either of two final patterns if one considers the number of spikes in the last layer: one having very few neurons firing (almost full decay) and the other having a rich number of firing neurons (nearly full firing). Litvak et al. (2000) argued that in a long feedforward network with excitatory–inhibitory balance, the activity after many layers is independent of the activity at the first layer, concluding that it is not possible to reliably transmit firing rates. If this is the case, the synchrony of firing is achieved at the expense of information loss in the neural activity. The question is: are there alternative modes of operation that prevent this loss of information?

In this paper, we show that such alternative modes of operation do exist and are intimately related to the distribution of connecting weights. These modes would result in different attractor states. Here, by an attractor state we mean a fixed point in the number of activated neurons, a limit cycle, or a more complex state.

This paper is organized as follows. In Sect. 2, the structure of the network is introduced. In Sect. 3, in a fully synchronized and noise free condition, the various modes of pattern propagation in such networks are classified and studied by numerical examples. In Sect. 4, a computer simulation is presented and compared with the theoretical results. By means of the simulation, the results are generalized to the more realistic case by incorporating a spontaneous neural activity and temporal asynchrony. In Sect. 5, the implications of this work and also conditions for preventing information loss are discussed.

2 The integrate-and-fire feedforward network

The network studied in this article is a multilayered, feedforward network, consisting of IFN models. The number of neurons in all layers is assumed to be equal.

2.1 The neuron model

The IFN model is a simplified approximation to the Hodgkin–Huxley neuron model (Koch 1999). The voltage of the IFN changes continuously as a function of its input, with the rate adjusted to the real neuron's membrane time constant. Whenever this continuous changing potential reaches a certain value (the threshold), an action potential is artificially inserted, which simulates the firing event. This is one of the shortcomings of the IFN compared with the Hodgkin–Huxley neuron model. Nevertheless, the IFN model is much more realistic than the classic binary (Ising) neuron models in which the states of the neuron are discrete.

2.1.1 The voltage dynamics. Assuming that the resting voltage of the IFN is zero, its voltage varies with time according to the following equation:

$$\frac{\mathrm{d}V_i^{\mu}}{\mathrm{d}t} = \frac{-V_i^{\mu} + \mathrm{Input}_i^{\mu}(t)}{\tau} \quad , \tag{1}$$

where V_i^{μ} is the voltage of the ith neuron at layer μ, τ is the time constant of the neuron which is taken equal for all the neurons in the network, and $\mathrm{Input}_i^{\mu}(t)$ is the incoming input to the ith neuron at layer μ.

2.1.2 Input. Except for the first layer, the input of each neuron is the weighted sum of the outputs of neurons in the previous layer, as illustrated in the following formula:

$$\mathrm{Input}_i^{\mu}(t) = \sum_j w_{ij}^{\mu}\, \mathrm{Output}_j^{\mu-1}(t - t_{ij}^{d}) \quad , \tag{2}$$

in which w_{ij}^{μ} is the weight of the connection between the jth neuron of the donor layer (layer $\mu - 1$) to the ith neuron of the recipient layer (layer μ), $\mathrm{Output}_j^{\mu-1}$ is the spike generated by the jth neuron of donor layer (layer $\mu - 1$), and t_{ij}^{d} is the connection delay.

For the case of simplicity, in this section we assume that the network operates in a noise-free condition and the neurons of the first layer are fed by a fully synchronous external input, which makes a certain proportion of them fire *simultaneously*. As will be shown in Sect. 4, the results obtained by this assumption are generalized to the case in which the feeding input is not synchronous.

2.1.3 Output. A constant threshold value is assigned to each IFN, which does not vary in time. The thresholds of the neurons in the network are normally distributed with $\overline{\mathrm{th}}$ and σ_{th}, as their mean and standard deviation, respectively. Whenever the membrane voltage of a neuron reaches its threshold, it fires; i.e., generates a spike which can be represented mathematically by a delta (impulse) function as

$$\mathrm{Output}_j^{\mu}(t) = \delta(t - t_{0j}^{\mu}) \quad , \tag{3}$$

where t_{0j}^{μ} is the firing time of the neuron, i.e., the time when its voltage has reached the threshold. Immediately after firing, the voltage of the neuron is rendered zero. In real neurons the duration of an effective action potential is short, so the above assumptions on the firing state (namely setting voltage to zero and using δ (an impulse function) as the ultimate output function) seem to be relevant.

2.2 Connections

The neurons within two successive layers are fully interconnected but there is no connection within a layer itself. There is also no feedback connection from one layer to the previous layers. All synaptic weights of the network are constant and distributed normally with mean weight of $\bar{w}$ and standard deviation of σ_w. When $\bar{w}$ is positive and the distribution is wide, some weights fall into the negative domain, hence the system contains both positive and negative weights. Conversely, if $\bar{w}$ is negative and its distribution increases, some weights fall into the positive domain. In either case, the inhibitory excitatory connections will be (partially) balanced.

As (1) shows, the IFN sums its inputs over time. Thus a more synchronized input results in a larger voltage in the neuron so that the ratio of firing neurons in a layer increases due to progressive synchronization and temporal summation, and we can be assured that this ratio will go on increasing, ending in the full activation of the final layers. Alternatively, if the input is not strong enough, this ratio will decline in successive layers, ending in total fading of the final layers. Hence, the very same condition that ensures synchrony causes information loss.

The important question is: Can one maintain synchrony and at the same time have sparse patterns of neurons fire in each layer, so that the final state is not independent of the initial state? The answer is that by adjusting the distribution of the weights this indeed is possible, and the above two scenarios are not the only possible alternatives.

3 Possible attractor states

Assuming that the connection delays are all equal and the feeding input is fully synchronized, the firing patterns of the successive layers remain fully synchronous and the connection delays have no effect in the number of firing neurons in successive layers. So, in order to simplify the analysis, we neglect the connection delays.

Assume $K = \{j_1, j_2, \ldots, j_{n^{\mu-1}}\}$ to be the set of the firing neurons in layer $\mu - 1$, where $n^{\mu-1}$ is the number of firing neurons in layer $\mu - 1$. Now, we omit the term t_{ij}^d from (2) and the term t_{0j}^μ from (3), and simply use t_0 to represent both of them. By merging (1), (2), and (3) and solving the resulting differential equation, the voltage of neuron i in layer μ can be calculated as

$$V_i^\mu(t) = \frac{\left(\sum_{j\in K} w_{ij}^\mu\right)}{\tau} e^{(t_0-t)/\tau} \cdot \theta(t - t_0) \ . \tag{4}$$

Evidently, the maximum voltage for the neuron is achieved at $t = t_0$, so that

$$V_{\max i}^\mu = \frac{1}{\tau} \cdot \sum_{j\in K} w_{ij}^\mu \approx \frac{n^{\mu-1} \cdot W_i^\mu}{\tau} \ , \tag{5}$$

where W_i^μ is the average of the incoming weights from the previous layer to the ith neuron at layer μ. Given that the weights of the network obey a normal distribution with mean $\bar{w}$ and standard deviation σ_w, the W_i^μ will obey a normal distribution with mean $\bar{w}$ and standard deviation $(\sigma_w/\sqrt{n^{\mu-1}})$. So, by (5) it is obvious that $V_{\max i}^\mu$ has in turn a normal distribution with mean $\overline{V_{\max}} = \frac{(n^{\mu-1}\cdot\bar{w})}{\tau}$ and standard deviation $\sigma_{V\max} = (\sqrt{n^{\mu-1}}\sigma_w)/\tau$. Clearly, if $V_{\max i}^\mu$ of the ith neuron is greater than its threshold, it will fire. In order to perform a comparison between the thresholds and the $V_{\max}$ over a layer, we introduce the following variable F:

$$F^\mu = V_{\max}^\mu - \mathrm{th} \ ,$$

which also obeys a normal distribution with mean

$$\overline{F^\mu} = \overline{V_{\max}^\mu} - \overline{\mathrm{th}} \ , \tag{6}$$

and variance

$$\sigma_{F^\mu}^2 = \sigma_{V_{\max}^\mu}^2 + \sigma_{\mathrm{th}}^2 = \frac{n^{\mu-1}\sigma_w^2}{\tau^2} + \sigma_{\mathrm{th}}^2 \ . \tag{7}$$

The number of firing neurons in layer μ (i.e., n^μ) could be calculated as follows:

$$n^\mu = N \cdot P(F^\mu > 0) \ , \tag{8}$$

where $P(F^\mu > 0)$ denotes the probablity of F^μ being positive, and N is the total number of the neurons in each layer. By standardizing the variable F as u:

$$u = \frac{F^\mu - \overline{F^\mu}}{\sigma_{F^\mu}}, \quad u_0 = \frac{-\overline{F^\mu}}{\sigma_{F^\mu}} = \frac{\tau \cdot \overline{\mathrm{th}} - n^{\mu-1} \cdot \bar{w}}{\sqrt{n^{\mu-1} \cdot \sigma_w^2 + \tau^2 \cdot \sigma_{\mathrm{th}}^2}} \ , \tag{9}$$

we find the number of firing neurons in layer μ to be

$$n^\mu = N \int_{u_0}^{+\infty} G(u)\mathrm{d}u \ , \tag{10}$$

where $G(u)$ is the standard normal distribution function. Finally, the relation between the numbers of firing neurons in two successive layers can be obtained as

$$n^\mu = N - N \int_{-\infty}^{u_0} G(u)\mathrm{d}u = R(n^{\mu-1}) \ . \tag{11}$$

It can be seen that the number of firing neurons in each layer is a function of the firing neurons in the previous layer. So, for calculating the number of firing neurons in successive layers one can iterate the function R on itself.

For simplicity of analysis, it is appropriate to assume that the function $R(n)$ admits a fixed point at $n \approx 0$ (i.e., if no neurons fire in one layer, also no neuron should fire in the next layer). This can be achieved if $\overline{\mathrm{th}} \gg \sigma_{\mathrm{th}}$. Using thresholds with means that are 3 times greater than their standard deviations will suffice. For the following numerical examples, we set the parameters to $\tau = 10$ ms, $\overline{\mathrm{th}} = 6$ mV, $\sigma_{\mathrm{th}} = 2$ mV, and $N = 50$.

3.1 Saturation and full decay

Given that $n \approx 0$ is a fixed point of $R(n)$, if $R'(n)$ near 0 is less than 1, then $n \approx 0$ will be an attractor; otherwise it will be a repeller. Due to approximations used in obtaining $R(n)$, $R'(n)$ at 0 is not well defined. In order to have an estimate for $R'(n)$ near 0, we have used $R'(1)$ instead. By some reasonable approximations based on assuming $\bar{w} \ll \tau \cdot \overline{\mathrm{th}}$, $\overline{\mathrm{th}} = 6$ mV and $\sigma_{\mathrm{th}} = 2$ mV, which applies in cases 1–3 below and case 1 of Sect. 3.2 we have found that $R'(1)$ will be less than 1 if

$$\frac{\sigma_w}{\tau\sigma_{\mathrm{th}}} < \frac{c_1}{N} \ , \tag{12}$$

otherwise $R'(1)$ will be more than 1. The constant c_1 depends weakly on the parameters of the model and is approximately 20 for the range of parameters chosen here. Before going further, it is worth noting that in the case of positive $\bar{w}$, $R(n)$ is a monotonic function for $0 < n \leq N$. Therefore $R'(n)$ near $n \approx 0$ predicts the slope at intersection (if any) to be greater than or lower than unity.

In the case that $R'(1) < 1$, i.e., $n \approx 0$ is an attractor, three different types of dynamical behavior of the function $R(n)$ are distinguishable; these are graphically represented in Fig. 1:

1. By the above argument, when $R(n)$ at $n \approx 0$ has an attractor and other fixed points exist, the next one will be a repeller. An example of this condition is $\bar{w} = 0.003$ mV · s and $\sigma_w = 0.001$ mV · s, in which the function has three fixed points; two attractors near 0 and N and a repeller in-between (Fig. 1a). In this case, if the feeding input of the network has lower number of firing neurons than the critical number given by the repeller, the firing state of the network will end up in full decay pattern in the tailing layers. But if the number of firing neurons in the feeding input is greater than the critical value, it will tend to saturation (full-firing state).

2. By decreasing $\bar{w}$ to 0.002 mV · s, the fixed points reduce to two; an attractor near zero and an unstable attractor near N, which acts as an attractor from the right side and as a repeller from the left side (Fig. 1b). That is, when the network is fed by an input having less firing neurons than this critical number, the firing state of the ending layers will tend to full decay, while when feeding it with an initial input having greater than the critical number of firing neurons, the number of firing neurons in the successive layers will tend to that critical value. However this point is unstable, and a small fluctuation may take the network toward its fixed point at zero.

3. By further decreasing $\bar{w}$, only one attractor fixed point will remain at $n \approx 0$ (Fig. 1c). In this case, the network results in a total fade state, regardless of the number of firing neurons in the input layer.

3.2 Existence of attractors at intermediate spike numbers

Considering the sign of $\bar{w}$, two situations can occur in this case:

1. When $\bar{w}$ is positive ($\bar{w} = 0.003$ mV · s in this example), considering (9) and (11), by increasing σ_w the slope of $R(n)$ at 1 will become greater than 1, and the situation described in case 1 of Sect. 3.1 changes to a new one. This transition occurs when $(\sigma_w/\tau\sigma_{\text{th}}) \approx (c_1/N)$ and *scales with N* (see Eq. 12). In other words, depending on the total number of neurons in each layer of the network, the transition occurs. In the example presented here, the transition occurs at $\sigma_w = 0.015$ mV · s (Fig. 2a). In this new situation, the function $R(n)$ has two fixed points, one at $n \approx 0$ and the other one which is an attractor. Note that in this case, by further increasing σ_w the attractor shifts to smaller values (Fig. 2b).

2. When $\bar{w}$ is negative, considering (9) and (11), the derivative of $R(n)$ will be negative. Also in this case two fixed points exist, a repeller at $n \approx 0$ and the other at intermediate values, say n_0. By some reasonable

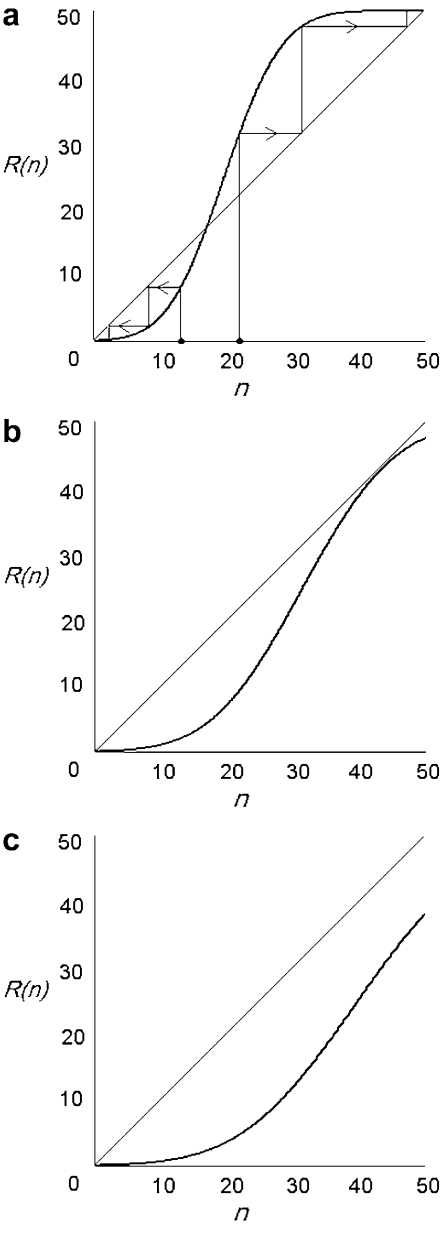

Fig. 1. Graph of the relation between the number of firing neurons in two successive layers ($R(n)$) versus the number of firing neurons in the previous layer (n). **a** $\bar{w} = 0.003$ mV · s, $\sigma_w = 0.001$ mV · s, The iterative mapping is shown by *arrows*. For these parameters, depending on the input pattern, the network has two final patterns (attractor fixed points) which are full firing or total decay. If the number of firing neurons in the input layer is greater or less than the unstable fixed point (the intersection of the curve $R(n)$ with the line $n = R(n)$ (the diagonal) in the *middle*), full firing or total decay pattern will result, respectively. **b** $\bar{w} = 0.002$ mV · s, $\sigma_w = 0.001$ mV · s. The graph of $R(n)$ tangents to the line $n = R(n)$. The fixed point near $n = 45$ has now become unstable, whereas the fixed point at the origin has remained stable. **c** $\bar{w} = 0.015$ mV · s, $\sigma_w = 0.001$ mV · s. Here the only fixed point is at $n \approx 0$. This means that the final pattern, independent of the input, is total fading

approximations, the condition for the intermediate fixed point to be an attractor ($R'(n_0) > -1$) is

$$\frac{\bar{w}}{\sigma_w} > \frac{c_2}{\sqrt{N}} \quad . \tag{13}$$

The constant c_2 is approximately -3.8 and is weakly dependent on the other parameters in the range we have chosen. Here again, the transition point *scales* with N; if N increases, with the same $\bar{w}$ one must increase σ_w to maintain the intermediate attractor. For the example presented here, the above condition will be fullfilled if $\bar{w} = -0.3$ mV · s and $\sigma_w = 0.64$ mV · s (Fig. 2c). Increasing σ_w causes the attractor to shift towards larger values.

With such parameters, the number of firing neurons in the tailing layers of the network will converge to a fixed value, regardless of the number of firing neurons in the feeding input. This does not mean there is a unique final pattern for the network in this condition (see Sect. 5). Note that the above condition is insensitive to the threshold distribution parameters. However, if the magnitude of the thresholds become many orders larger ($\overline{\text{th}}$ or $\sigma_{\text{th}} > (\bar{w} \cdot N/\tau)$), the above condition will change.

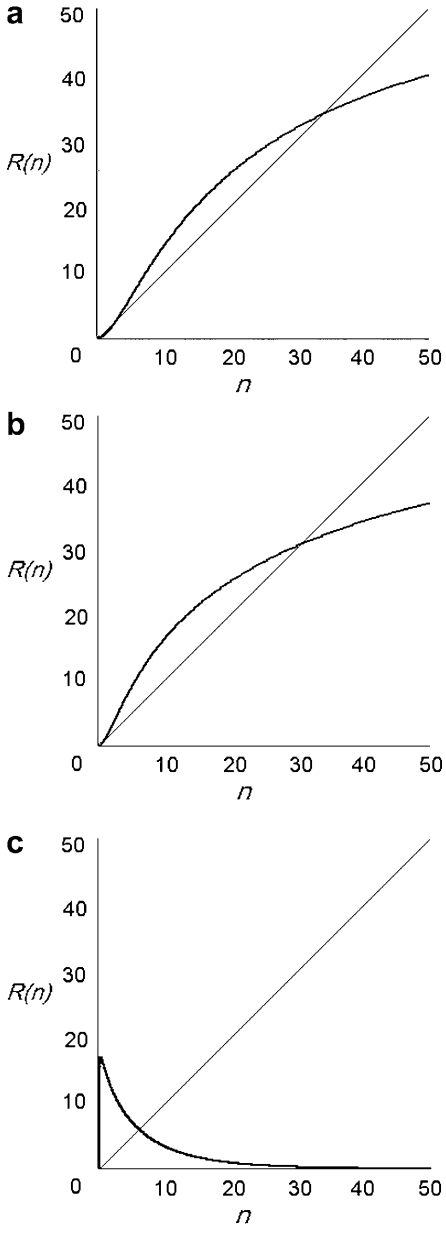

Fig. 2a–c. Graph of $R(n)$ versus n for larger values of σ_w. **a** $\bar{w} = 0.003$ mV · s, $\sigma_w = 0.015$ mV · s. The network has an attractor fixed point. Comparing with Fig. 1a, this demonstrates the transition phase of the network. So that except for the input patterns with a very small number of firing neurons, other inputs will result in final patterns near the attractor fixation point. **b** $\bar{w} = 0.003$ mV · s, $\sigma_w = 0.02$ mV · s. The transition phase has passed. Here, independent of the input pattern, the final layers have patterns with number of firing neurons near the attractor fixed point. **c** $\bar{w} = -0.3$ mV · s, $\sigma_w = 0.64$ mV · s. Another parametrization of the network, leading to a fixed point. Here the negative weights (inhibitory connections) are balanced by widening of the distribution

3.3 Fluctuation between states with different numbers of firing neurons

It is possible that the number of firing neurons never converges to a fixed number, but fluctuates and never ends up in full firing or in total decay. This condition will be achieved if $R(n)$ has a cycle attractor. This is the case when the function $y = R(n)$ intersects the line $y = x$ with a slope less than -1 (Fig. 3b). Considering (13), the condition for the slope in the intermediate fixed point to be less than -1 is

$$\frac{\bar{w}}{\sigma_w} < \frac{c_2}{\sqrt{N}} \quad . \tag{14}$$

So by decreasing σ_w (when $\bar{w}$ is fixed at -0.3 mV · s in this example), the slope of the function $R(n)$ at the non-zero fixed point decreases and consequently becomes less than -1 (when σ_w becomes less than 0.6 mV · s) and the situation described in case 2 of Sect. 3.2 changes. Then, in the new situation, the function $R(n)$ will have a cycle or possibly a strange attractor; that is, the number of firing neurons in the successive layers of the network will fluctuate between various values, either periodically (see Fig. 3a) or in a multiple periodic/chaotic manner (see Fig. 3b).

The changes in the network dynamical states as a function of σ_w are summarized in a bifurcation diagram shown in Fig. 4. This figure demonstrates the borders of the network dynamics transition from convergence to a single attractor to a cycle attractor (at $\sigma_w = 0.10$), from cycle attractor to strange (chaotic) attractor (at $\sigma_w = 0.12$), from strange (chaotic) attractor to cycle attractor again (at $\sigma_w = 0.27$), and finally from cycle attractor to point attractor (at $\sigma_w = 0.59$). The above numeric examples (from case 2 of Sect. 3.2 onwards) for each behavior clearly lies between these borders and are shown by arrows in Fig. 4. The figure also shows – in many interesting cases (limit cycles with a period more than two and chaotic behavior) – that many of the attractor points are less than one. As the number of the neurons is a discrete value, some of these attractor points will be truncated to zero in a real network and the

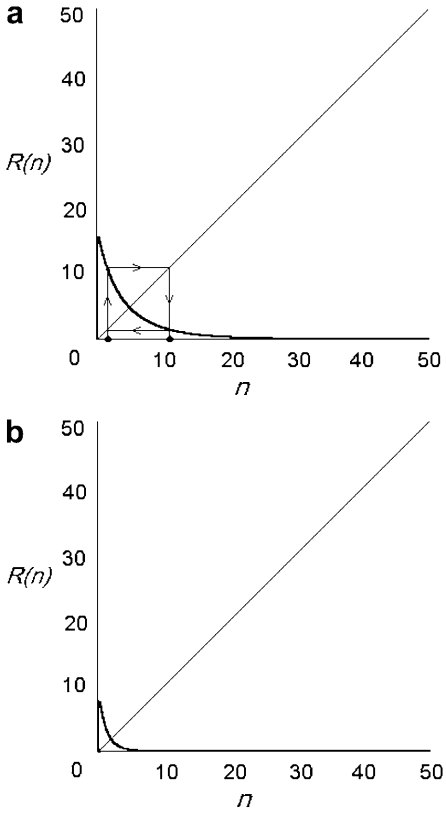

Fig. 3a,b. Graph of $R(n)$ versus n for negative values of $\overline{w}$. **a** $\bar{w} = -0.3$ mV · s, $\sigma_w = 0.528$ mV · s. Comparing with Fig. 2c, the R(n) curve intersects the $n = R(n)$ line with a slope less than -1, so here – as illustrated by the iterative map (*arrows*) – the network has a period-2 attractor. The simulation result (Fig. 5e) as well as the bifurcation diagram (Fig. 4) show that the number of firing neurons in successive layers oscillates between two values. **b** $\bar{w} = -0.3$ mV · s, $\sigma_w = 0.256$ mV · s. Also in this case, the slope of the curve at the intersection with the line $n = R(n)$ is less than -1, so cyclic or possibly chaotic behavior will be expected. The bifurcation diagram (Fig. 4) and the simulation results confirm this expectation, showing oscillation between more than two values. In this case, the number of firing neurons in the in final layers fluctuates, resulting in richer possible patterns

network will be trapped in full fading (because $n = 0$ is a fixed point). So it is predictable that we cannot see a long-lasting multiple periodic/chaotic behavior in the simulation in a noise-free condition. But as we will show in Sect. 5, the presence of a finite amount of inherent noise prevents the network from being trapped in the full fading condition, and a long-lasting multiple periodic/chaotic behavior is possible.

4 Simulation

We assess the above discussion through a computer simulation that was performed on a PC using the Delphi 5 programing language.

In our simulation we studied the time-dependent behavior of a multilayered, feedforward network of IFNs. This network has 20 layers, each connected to the next layer. There are 50 neurons in each layer. Intralayer connections and feedbacks do not exist. The model used

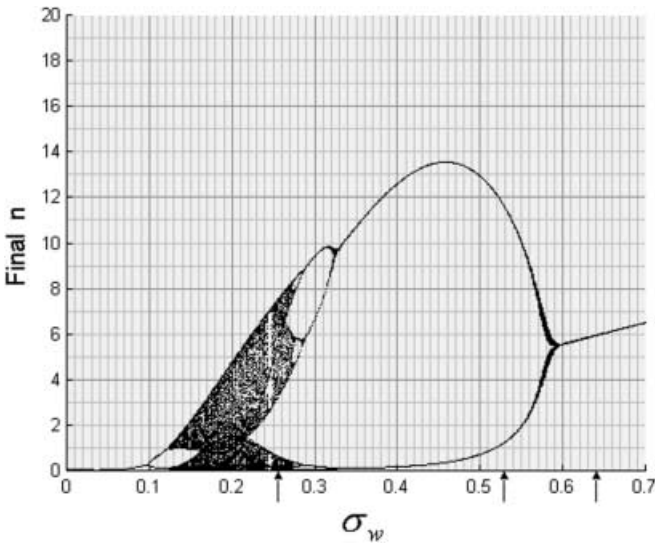

Fig. 4. By fixing $\bar{w}$ at -0.3 mV · s, σ_w is changed from 0 to 0.7 to obtain the bifurcation diagram. The *horizontal axis* shows the value of σ_w and *vertical axis* represents the possible numbers of firing neuron in the tailing layers (attractors). For $0 < \sigma_w < 0.1$, the system has a single point attractor near zero. For $0.1 < \sigma_w < 0.12$, cycle attractors exist. For $0.12 < \sigma_w < 0.27$, the system has multiple periodic/chaotic attractors. For $0.27 < \sigma_w < 0.59$, the cycle attractors reappear. And for $0.59 < \sigma_w$, we have a single point attractor again. The different examples of the corresponding values of σ_w, which are discussed in the following demonstrations, are shown with *arrows* here. This curve is drawn analytically using the assumption that the network is noise free and the input is fully synchronized

for the neuron is an integrate-and-fire model. The forward Euler method is used to integrate the differential equations in fixed time steps of 0.1 ms. The weights and the thresholds are drawn from a Gaussian distribution using a pseudorandom number generator. At the beginning of each run, a number of neurons in the input layer fire either simultaneously or with a time standard deviation of 3 ms (Diesmann et al. 1999). We then monitor the progress of the firing patterns in the network.

4.1 Simulation results in the noise-free and synchronous condition

Figure 5 shows the results of our simulation for the above-mentioned parameters, which correspond to Figs. 1–3. It is worth remembering that in the figures discussed in the previous sections, the function $R(n)$ was plotted, which maps the number of firing neurons in one layer to the number of the firing neurons in its next layer. However, in Figs. 5–7, in order to show the dynamic behavior of the simulated network explicitly, the number of firing neurons in each layer is plotted versus the layer number. Note that $R(n)$ represents an average behavior of the network, which is in fact a mean field approximation to the network, whereas the simulations were run for ten samples of parameter values and connections. This shows that the analysis is robust, and when large number of neurons is involved the predicted behavior will be observed.

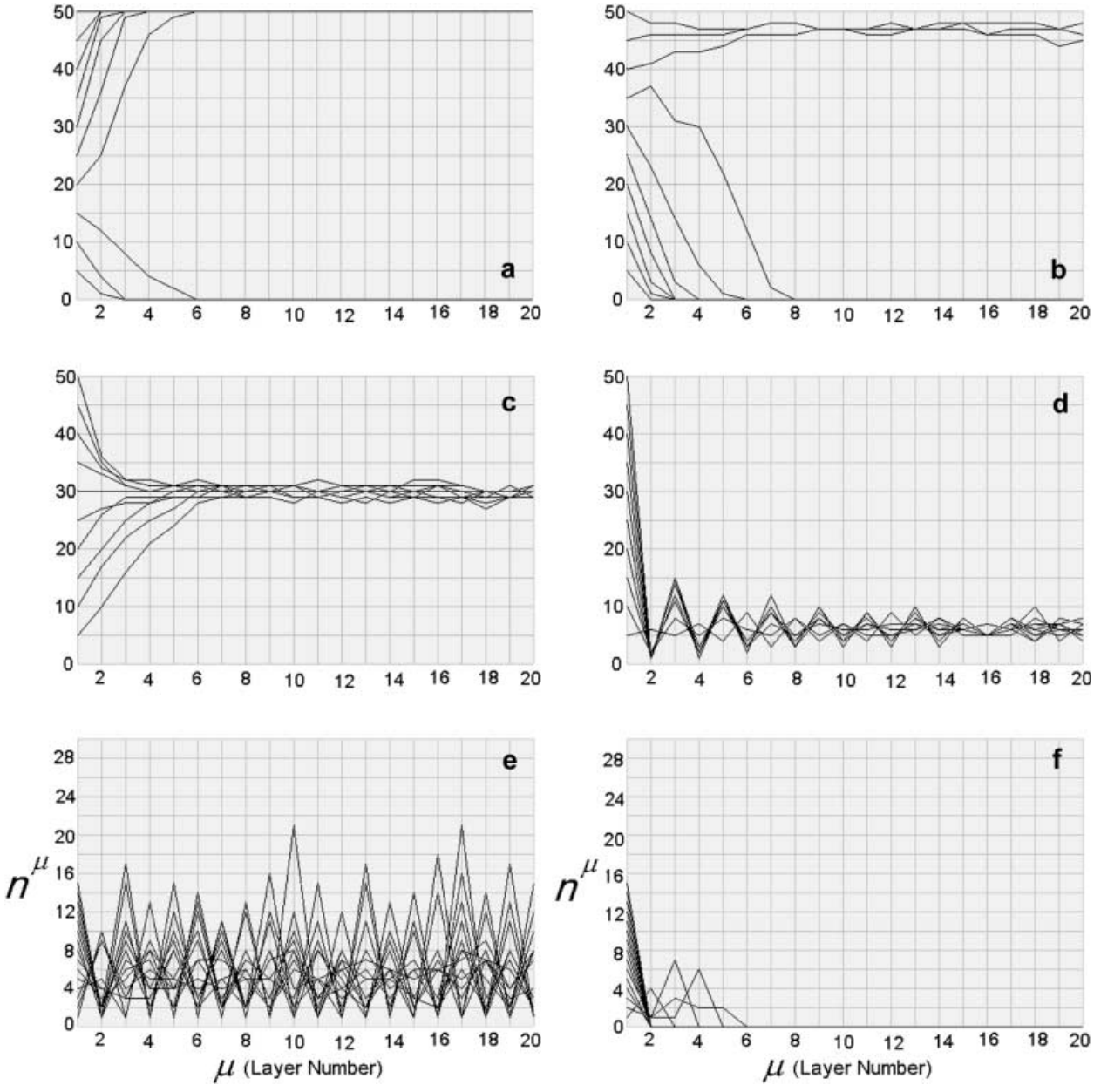

Fig. 5a–f. Inputs with different numbers of firing neurons are traced up to the last layer by means of the simulation. The graphs are results of ten realization of the network with the corresponding parameters. **a** $w = 0.003$ mV · s and $\sigma_w = 0.001$ mV · s, corresponding to Fig. 1a. Depending on the input, full firing or total fade occurs. So the output has only two possible patterns. **b** $w = 0.002$ mV · s and $\sigma_w = 0.001$ mV · s, corresponding to Fig. 1b. Depending on the input, the state (pattern) progression differs. If the number of firing neurons in the input layer exceeds a critical value (the tangent point in Figure 1b) the network tends to an attractor state near full firing. On the other hand, if the input number of firing neurons is less than the critical value, the situation is the same as the total fading state. **c** w = 0.003 mV · s and $\sigma_w = 0.02$ mV · s, corresponding to Fig. 2b. Independent of firing number in the input, the patterns in successive layers have the same range of firing number. A full-firing input does not result in the full-firing state, and inputs with few firings do not end up in total fade. This is a suitable network dynamic for producing a rich number of output patterns. **d** $w = -0.3$ mV · s and $\sigma_w = 0.64$ mV · s, corresponding to Fig. 2c. Convergence to a range of firing numbers is seen. The main difference with previous case is that we have more fluctuations. This is because the curve $R(n)$ intersects the line $n = R(n)$ in a negative slope, so convergence to the fixed point is achieved through diminishing cyclic patterns (which can be traced well in the dentate shape of this curve). The inputs with more firings result in less firing pattern in the second layer, and vice versa. **e** $w = -0.3$ mV · s and $\sigma_w = 528$ mV · s, corresponding to Fig. 3a. The state of the network finds a cyclic character and does not converge to a fixed point. Note the oscillations in successive layers between 1 and 11. In this system some input states fade. Those which do not, end up to either 1 or 11 firing neurons in the final layer. This does not mean there are only two final patterns; rather, a large number of patterns is possible (see Sect. 5). **f** $w = -0.3$ mV · s and $\sigma_w = 0.256$ mV · s, corresponding to Fig. 3b. In this case although the bifurcation diagrams shows a multiple periodic or chaotic behavior, this behavior cannot survive for a long range in the simulation (see Sect. 3.3)

Figure 5a shows the result of the simulation for the situation described in case 1 of Sect. 3.1. As expected, when the number of firing neurons in the first layer is less than the intermediate fixed point, there will be no firing neuron in the last layers; i.e., a full decay condition occurs. But when the number of firing neuron in input layer exceeds the intermediate fixed point, the full-firing state appears in the tailing layers. In case 2 of Sect. 3.1, a transitional phase was described. As can be seen in Fig. 5b, the simulation shows the semi-attractor/semi-repeller behavior of the described fixed point clearly.

The simulation result for the behavior discussed in Sect. 3.2 is shown in Fig. 5c and d. In these cases, for any input pattern the number of firing neurons in the last layer converges to a fixed value. Note that there is a slight difference between the behaviors of the network when it has a positive mean weight (Fig. 5c) compared to when it has a negative mean weight (Fig. 5d). In the former condition, the convergence of the number of the firing neurons to the fixed point has occurred somehow monotonically, while in the latter condition, the convergence to the fixed point progresses with a diminishing fluctuation.

When the conditions described in Sect. 3.3 are imposed on the simulated network, for $w = -0.3\ \mathrm{mV} \cdot \mathrm{s}$ and $\sigma_w = 528\ \mathrm{mV} \cdot \mathrm{s}$, the predicted fluctuation of the number of firing neurons between two values (about 1 and 11) in successive layers can be observed without any convergence to a fixed value, hence indicating a cycle attractor with period two (see Fig. 5e). But for $w = -0.3\ \mathrm{mV} \cdot \mathrm{s}$ and $\sigma_w = 256\ \mathrm{mV} \cdot \mathrm{s}$, a very short-range fluctuation of the number of firing neurons can be observed, as predicted in Sect. 3.3 (see Fig. 5f).

4.2 Cases in which noise and asynchrony exist

So far we have analyzed and simulated the network in a noise-free mode, fed by synchronous input. It is an important question as to what will happen to the dynamics if:

1. One feeds the network with asynchronous input.
2. The neurons have an inherent noise.

This will be discussed in this section.

4.2.1 Saturation and full decay. We fed the network with input patterns having a time standard deviation of 3 ms. As before, we traced the number of firing neurons (as well as the standard deviation of each layer with time) in the successive 20 layers. A number was assigned to each layer, which is the average number of firings in 10 network realizations:

1. Figure 6a shows the asynchronous case of "saturation and full decay" (case 1 of Sect. 3.1) with weight parameterization chosen similar to Fig. 5a. There is no important modulation but a slower move toward full firing and more rapid progression toward full decay. The synchronization in case of full firing is achieved in a few layers of propagation (not shown). The very same case then was investigated when each neuron spontaneously produces spikes in a Poisson manner with a mean frequency of 2 Hz, in additon to the spikes due to their membrane potential dynamics (see Fig. 7a). It is interesting to note that full saturation becomes much more rapid; also, full decay is not stable. This is explained by the ability of noise to prevent the full fading of neurons and to excite them to produce spikes even in the state of full fading. The agile movement toward full firing can be explained by the assistance of noise (spontaneous spikes) in exciting more neurons in each successive layer, hence resulting in more rapid full firing. This result is in agreement with the study of Diesmann et al. (1999). Nevertheless, gradual movement toward synchrony is observed and the time standard deviation of firing patterns decreases and reaches a non-zero baseline (not shown).

2. Figures 6b and 7b demonstrate simulation results for the case 2 of Sect. 3.1 in an asynchronously fed network and noisy conditions. In these cases, no informative state remains, i.e., full fading results regardless of input. Even noise cannot change the dynamics toward the stabilization, but merely prevents the network from falling into absolute decay and a noise-dependent uncorrelated activity finally remains.

4.2.2 Convergence to a fixed number of firing neurons. Now we turn to the case where the network reaches a stable state, as discussed in Sect. 3.2. Is this dynamic robust against asynchrony and noise?:

1. Figure 6c shows the fixed-point convergence behavior (weight parameters as in case 1 of Sect. 3.2) when the input is asynchronous but noise is absent. Again the numbers converge and synchronization is achieved after a few layers (not shown). Figure 7c demonstrates the same condition with noise. Here the number of firing neurons in the first few layers is higher than the noise-free case. The number of firings gradually shifts toward the stable state, but this is still higher than in the noise-free case.

2. Figure 6d shows the fixed-point convergence behavior (weight parameters as in case 2 of Sect. 3.2) when the input is asynchronous but noise is absent. Here again, with negative mean weight the firing numbers tend to a fixed value. The second layer gains a larger number of firings compared with the synchronous case in Fig. 5d. In the presence of noise (see Fig. 7d), the fluctuations are more irregular but the convergence behavior still exists. It is worth noting that gradual synchronization also occurs in this condition (not shown).

4.2.3 Fluctuation between patterns with different numbers of firing neurons. Figure 6e shows the network behavior for $w = -0.3\ \mathrm{mV} \cdot \mathrm{s}$ and $\sigma_w = 0.528\ \mathrm{mV} \cdot \mathrm{s}$, with an asynchronous input and in the absence of noise. As in the synchronous case in Fig. 5e, cyclic behavior is observed, but the second layer exhibits a greater number of firings. Figure 7e shows the same condition in the presence of noise. Note the larger amplitude of oscillation between two limits.

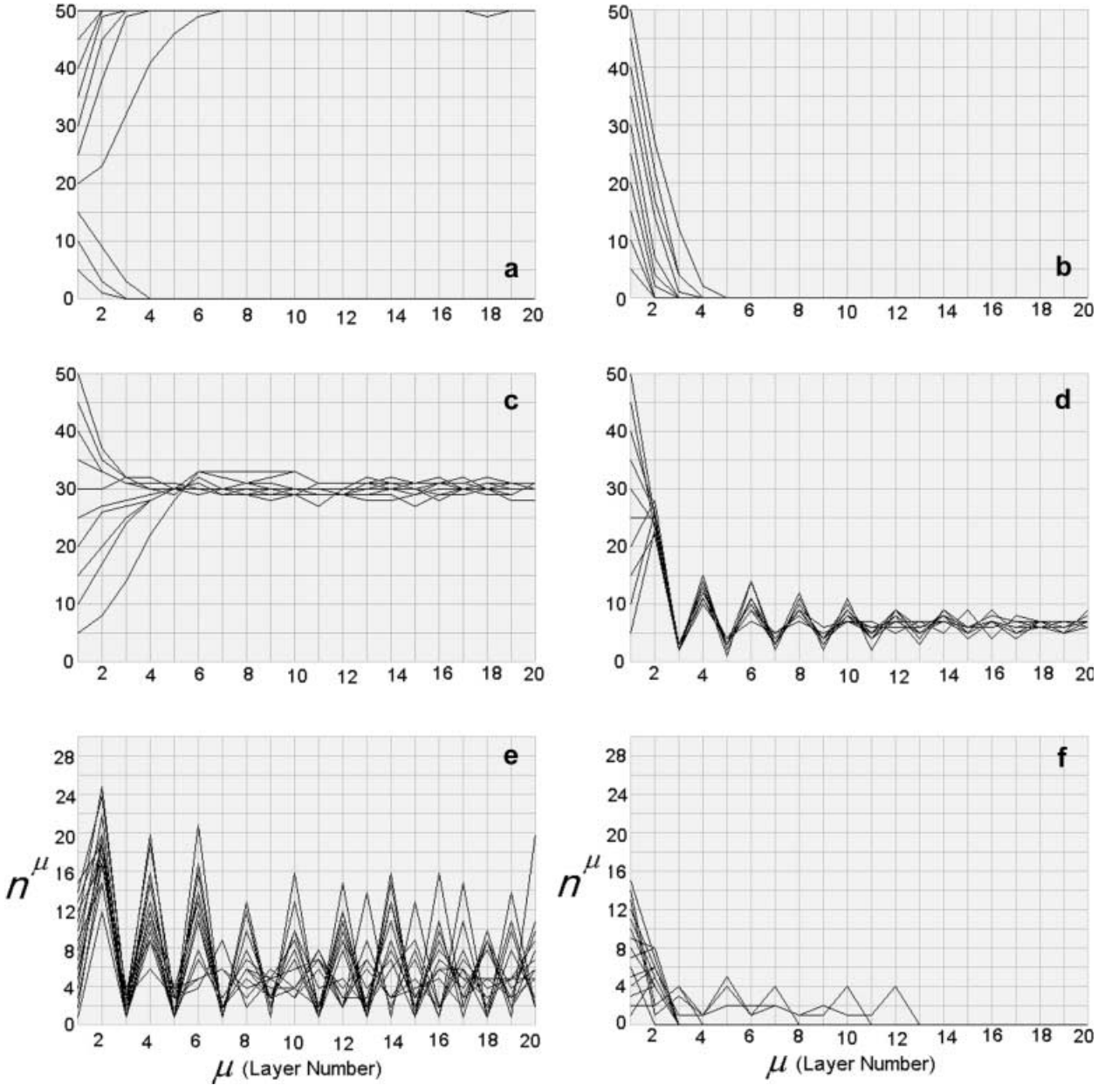

Fig. 6a–f. The simulation results for the same parameters as for Fig. 5, but with an asynchronous input pattern having a time standard deviation of 3 ms. **a** $w = 0.003$ mV · s, $\sigma_w = 0.001$ mV · s. Feeding the network with an asynchronous input does not change the dynamic behavior of the firing state, and the full-firing or full-decay behavior remains. **b** $w = 0.002$ mV · s, $\sigma_w = 0.001$ mV · s. In this case the asynchrony of the feeding input causes the network to end up in full fade, regardless of the number of firing neurons in the feeding input. **c** $w = 0.003$ mV · s, $\sigma_w = 0.02$ mV · s. The asynchronous feeding input does not change the convergence behavior in this case. **d** $w = -0.3$ mV · s, $\sigma_w = 0.64$ mV · s. The asynchronous feeding input caused a rise in the number of firing neurons in the second layer, but the convergence behavior remains unchanged. **e** $w = -0.3$ mV · s, $\sigma_w = 0.528$ mV · s. The cyclic character survives in the case of an asynchronous input. Here also, an asynchronous input causes a rise in the number of firings in the second layer. **f** $w = -0.3$ mV · s, $\sigma_w = 0.256$ mV · s. As Fig. 5f, there is no long-range survival in the case of multiple periodic or chaotic behaviors. However, it lasts longer than the case of Fig. 5f

Figure 6f shows the network behavior for $w = -0.3$ mV · s and $\sigma_w = 0.256$ mV · s, with an asynchronous input and in the absence of noise. Comparing with the synchronous case in Fig. 5e, although the fluctuations survive longer, they also fade off finally in this case. As discussed in Sect. 3.3, this fading is due to truncation of the attractor values less than 1. Figure 7f demonstrates the network dynamics for the same weight parameters in the presence of noise plus a asynchronous input. It is important to note that in this condition, a long-lasting irregular (multiple periodic/chaotic) fluctuation can be observed. The reason for this long-lasting fluctuation is that noise cancels the truncation effect; i.e., noise reveals the multiple periodic/chaotic behavior of the network.

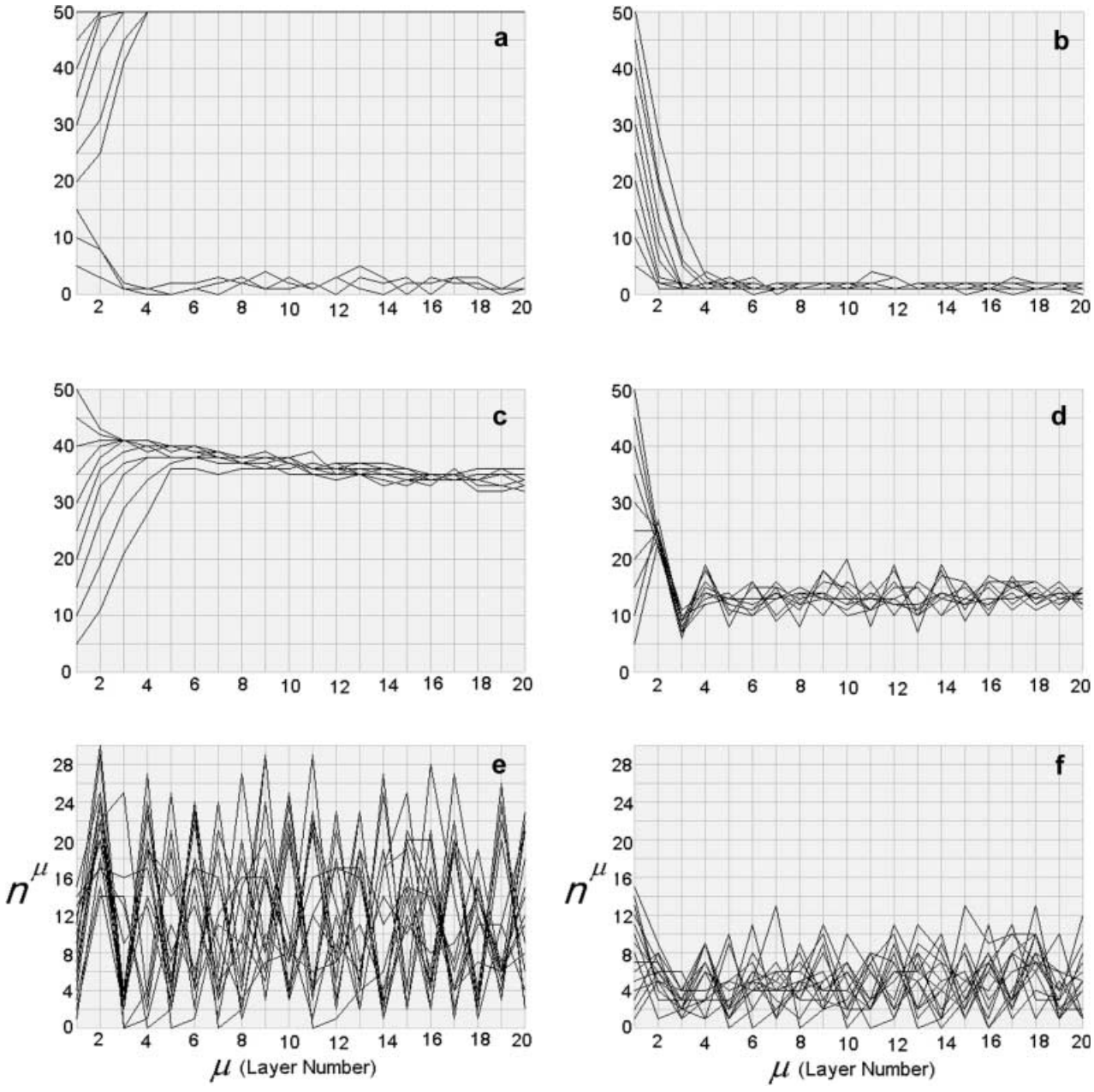

Fig. 7a–f. The simulation results for the same parameters as Figs. 5 and 6, with an inherent Poisson noise (spontaneous firing) of 2 Hz for each neuron in every layer. Again, the input pattern has a time standard deviation of 3 ms. **a** $w = 0.003$ mV · s, $\sigma_w = 0.001$ mV · s. The noise and asynchrony do not change the dynamic behavior of the number of the firing neurons, and the full firing or sparse uncorrelated behavior remains. **b** $w = 0.002$ mV · s, $\sigma_w = 0.001$ mV · s. In this case, despite the inherent noise of the neurons the asynchrony of the feeding input causes the network to end up in relative fading, regardless of the number of firing neurons in the feeding input. Due to noise, fading is not complete. **c** w = 0.003 mV · s, $\sigma_w = 0.02$ mV · s. The asynchronous feeding input plus noise does not change the convergence behavior in this case. But compared to Fig. 6c, the number of firing neurons in the heading layers is higher and tends to the attractor state gradually. **d** $w = -0.3$ mV · s, $\sigma_w = 0.64$ mV · s. Here also, the rise in the number of firing neurons in the second layer can be observed (compared to Fig. 5d, the convergence behavior remains unchanged except for its more irregular trend. **e** $w = -0.3$ mV · s, $\sigma_w = 0.528$ mV · s, cyclic character can be seen even when noise is added, however it is more irregular than both Figs. 5e and 6e. Also, here a rise in the number of firings in the second layer can be observed. The rise is more than the case in Fig. 6e. **f** $w = -0.3$ mV · s, $\sigma_w = 0.256$ mV · s. In contrast to Figs. 5f and 6f, a long-range survival of multiple periodic or chaotic behavior can be seen. Noise pushes the network from the full fade region (see Fig. 4) to reveal the multiple periodic or chaotic behaviors. In Figs. 5f and 6f, the network is entrapped in the values of n less than one, hence this must be a full fade, but the driving effect of noise prevents a full fade state. The observed irregularity of the propagation reveals the existence of multiple periodic or chaotic behaviors

5 Discussion

As discussed earlier, synchronized firing in each layer of a multilayered neural network either may produce powerful input for the next layer, causing a yet greater number of neurons to fire and thus creating the full firing state, or may not be able to produce a pattern strong enough to maintain the firing of the neurons in the next layers, causing an ultimate full decay. In both of these extreme conditions, information is lost.

Diesmann et al. (1999) have shown that the dynamical behavior of a feedforward integrate-and-fire network results in two attractors: near total fade or full firing states. This is similar to the results obtained in Sect. 4.2.1. However, we have shown (in Sects. 3 and 4) that by varying the distribution of the connection weights, the network can have attractor states which are different from the two extreme conditions. It is worth noting that our model is simpler than that of Diesmann et al. (1999). One major simplification is that we used an instantaneous response function (δ function) in the synapses (as Hermann et al. 1995; Hertz and Prügel-Bennett 1996; Marsalek et al. 1997; Koch 1999), while in Diesmann et al. (1999) the neurons have a finite voltage rise time in response to each incoming input spike (α function). The other simplification is that the noise we incorporated in the network (Sect. 4.2) is in the form of spontaneous activity; that is, in addition to the membrane potential dynamics, the neurons generate spikes at random times, resulting in a low-rate Poisson background activity; whereas in Diesman et al. (1999) a synaptic noise input is also present. The effect of these modifications on the network dynamics remains to be studied.

As we mentioned earlier, Litvak et al. (2000) have argued that in a long feedforward network of IFN models, because of the presence of shared inputs, one observes that the pattern of activity in the mth layer (if m is large enough) will be independent of the firing pattern with which the network has been fed. We emphasize here that the very means to avoid such undesirable behavior is to adopt one of the following strategies. First, if the total number of neurons in each pool is increased and the ratio of firing neurons remains fixed, the number of firing neurons in each layer will increase and thus a larger $\sigma_{V\max}$ is obtained (see Sect. 3) in following layers. Second, with a wider distribution of connecting weights or a smaller τ, one will certainly expect a larger $\sigma_{V\max}$ in the following layers. These strategies increase the possible firing patterns of each pool and make them more dependent on the input.

In this paper we have shown that such a network can have various modes of behavior depending on the distribution of its connection weights. In these cases, the existence of rich dynamics may allow informative processes to be carried out.

It is worth mentioning how information is contained in the firing pattern of a layer. Consider a layer of N neurons containing n firing neurons. This firing state can be of $\binom{N}{n}$ different patterns. So the information could be carried by the composition of the firing neurons, which make up the firing pattern. However, firing states consisting of N or 0 firing neurons (full-firing or total decay states) can have only one combinatorial pattern, and so are poor from the information content viewpoint. So when the number of neurons in the firing patterns of the network converges to an intermediate fixed point (as described in Sect. 3.2), they may contain information. The same is true for a cycle attractor. In the case of the multiple periodic/chaotic state, the network benefits from a finite amount of noise to reveal this rich behavior, which is hidden in the noise-free condition (see Sect. 4.2.3).

In the case of convergence to a fixed-point attractor state, depending on the number of firing neurons in the tailing layers (n), the number of all possible patterns in the last layer is $\binom{N}{n}$, while the number of all possible patterns in the first layer is 2^N. As $\binom{N}{n} < 2^N$, a kind of categorization of input into output may occur. In the case of limit cycles a similar analysis applies. Whether this kind of classification will be functional in practice requires further research; all that can be shown for now is the presence of some new attractors in synfire chains, which are different from the states of total decay and full activation found earlier by others.

Here we must note some of the limitations in generalizing the above results to the more complex models of the neural system. When trying to generalize these results to a network consisting of Hodgkin–Huxley neuron models, one must consider some differences between the IFN and the Hodgkin–Huxley neuron models. The IFN used in our model is an oversimplified model of the neuron, in which the different phases of activity (integration of the input and spiking) have been artificially separated and the threshold value is explicitly imposed in this model, while in the Hodgkin–Huxley model, different phases of activity are not separated and the threshold value is implicitly embedded in the equations. Hence, it does not seem to be straightforward to generalize our above analysis to the case in which the thresholds are not explicit values. However, when treating a single train of spikes in the network, our reasoning may not be impaired significantly, as the implicit thresholds can be assumed to be normally distributed.

We should also remind the reader that we did not generalize our analysis to the case in which the network is fed by a number of successive patterns instead of a single one. However, even with our simplified analysis it is clear that a feedforward integrate-and-fire network can transmit informative spike patterns, thus it can be trained for pattern processing applications. The proper learning algorithms for such a network remain to be studied in further investigations.

Acknowledgements. We thank A. Aertsen and J. Hertz for offering useful comments on the initial version of this article. We would also like to thank an anonymous reviewer for precise and helpful comments throughout the revision process.

References

Abeles M (1991) Corticonics: neuronal circuits of cerebral cortex. Cambridge University Press, Cambridge

Aertsen A, Diesmann M, Gewaltig MO (1996) Propagation of synchronous spiking activity in feedforward neural networks. J Physiol Paris 90: 243–247

Arnoldi HM, Brauer W (1996) Synchronization without oscillatory neurons. Biol Cybern 74: 209–223

Arnoldi HM, Englmeier KH, Brauer W (1999) Translation-invariant pattern recognition based on Synfire chains. Biol Cybern 80: 433–447

Burkitt AN, Clark GM (1999) Analysis of integrate-and-fire neurons: synchronization of synaptic input and spike output. Neural Comput 11: 871–901

Campbell SR, Wang DL, Jayaprakash C (1999) Synchrony and desynchrony in integrate-and-fire oscillators. Neural Comput 11: 1595–1619

Chawla D, Lumer ED, Friston KJ (1999) The relationship between synchronization among neuronal populations and their mean activity levels. Neural Comput 11: 1389–1411

Deco G, Schürmann B (1999) Spatiotemporal coding in the cortex: information flow-based learning in spiking neural networks. Neural Comput 11: 919–934

Diesmann M, Gewaltig M-O, Aertsen A (1999) Stable propagation of synchronous spiking in cortical neural networks. Nature 402: 529–532

Gerstner W, van Hemmen JL (1992) Universality in neural networks: the importance of the 'mean firing rate'. Biol Cybern 67: 195–205

Hansel D, Sompolinsky H (1996) Chaos and synchrony in a model of a hypercolumn in visual cortex. J Comput Neurosci 3: 7–34

Hansel D, Mato G, Meunier C, Neltner L (1998) On numerical simulations of integrate-and-fire neural networks. Neural Comput 10: 467–483

Herrmann M, Hertz JA, Prügel-Bennett A (1995) Analysis of synfire chains. Netw Comput Neural Syst 6: 403–414

Hertz J, Prügel-Bennett A (1996) Learning synfire chains: turning noise into signal. Int J Neural Syst 7: 445–450

Hopfield JJ, Herz AV (1995) Rapid local synchronization of action potentials: toward computation with coupled integrate-and-fire neurons. Proc Natl Acad Sci USA 92: 6655–6662

Horn D, Opher I (1997) Solitary waves of integrate-and-fire neural fields. Neural Comput 9: 1677–1690

Hummel JE, Biederman I (1992) Dynamic binding in a neural network for shape recognition. Psychol Rev 99: 480–517

Kempter R, Gerstner W, van Hemmen JL (1998) How the threshold of a neuron determines its capacity for coincidence detection. Biosystems 48: 105–112

Koch C (1999) Simplified models of individual neurons. In: Koch C (ed) Biophysics of computation: information processing in single neurons. Oxford University Press, Oxford

König P, Engel AK, Roelfsema PR, Singer W (1995) How precise is neuronal synchronization? Neural Comput 7: 469–485

Lachaux JP, Rodriguez E, Martinerie J, Varela FJ (1999) Measuring phase synchrony in brain signals. Hum Brain Mapp 8: 194–208

Lin JK, Pawelzik K, Ernst U, Sejnowski TJ (1998) Irregular synchronous activity in stochastically-coupled networks of integrate-and-fire neurons. Network 9: 333–344

Litvak V, Sompolinsky H, Segev I, Abeles M (2000) On the transmission of rate code in long feedforward networks with excitatory–inhibitory balance. In: Proceedings of the Computational Neuroscience Meeting, Brugge, Belgium, 16–20 July p 94

Lumer ED, Edelman GM, Tononi G (1997) Neural dynamics in a model of the thalamocortical system. II. The role of neural synchrony tested through perturbations of spike timing. Cereb Cortex 7: 228–236

MacGregor RJ, Ascarrunz FG, Kisley MA (1995) Characterization, scaling, and partial representation of neural junctions and coordinated firing patterns by dynamic similarity. Biol Cybern 73: 155–166

Marsalek P, Koch C, Maunsell J (1997) On the relationship between synaptic input and spike output jitter in individual neurons. Proc Natl Acad Sci USA 94: 735–740

Miller R (1996) Cortico-thalamic interplay and the security of operation of neural assemblies and temporal chains in the cerebral cortex. Biol Cybern 75: 263–275

Niebur E, Koch C (1994) A model for the neuronal implementation of selective visual attention based on temporal correlation among neurons. J Comput Neurosci 1: 141–158

Pinsky PF, Rinzel J (1995) Synchrony measures for biological neural networks. Biol Cybern 73: 129–137

Postma EO, van den Herik HJ, Hudson PT (1996) Robust feedforward processing in synfire chains. Int J Neural Syst 7: 537–542

Prut Y, Vaadia E, Bergman H, Haalman I, Slovin H, Abeles M (1998) Spatiotemporal structure of cortical activity: properties and behavioral relevance. J Neurophysiol 79: 2857–2874

Rudd ME, Brown LG (1997) Noise adaptation in integrate-and fire neurons. Neural Comput 9: 1047–1069

Somers D, Kopell N (1993) Rapid synchronization through fast threshold modulation. Biol Cybern 68: 393–407

Tal D, Schwartz EL (1997) Computing with the leaky integrate-and-fire neuron: logarithmic computation and multiplication. Neural Comput 9: 305–318

Usrey WM, Reid RC (1999) Synchronous activity in the visual system. Annu Rev Physiol 61: 435–456